ChemPubSoc Europe

DOI: 10.1002/cssc.201801432

CHEMSUSCHEM Communications

Realizing High-Performance Li–Polysulfide Full Cells by using a Lithium Bis(trifluoromethanesulfonyl)imide Salt Electrolyte for Stable Cyclability

Syed Abdul Ahad,[a, b] Ragupathy Pitchai,*[b, c] Anteneh Marelign Beyene,[b] Sang Hoon Joo,[a] Do Kyung Kim,*[b] and Hyun-Wook Lee*[a]

Since concentrated electrolytes have attracted great attention for the stabilization of lithium-metal anodes for lithium-ion batteries, the demonstration of a full cell with an electrolyte concentration study has become a research topic of interest. Herein, we have demonstrated a proof of concept, a lithium–polysulfide full cell battery using various lithium bis(trifluoromethanesulfonyl)imide (LiTFSI) electrolyte concentrations with glass-fiber-based composite and hard carbon as the cathode and anode, respectively. The initial capacity of the lithium-polysulfide full cell is found to be 970 mA h g^{-1} at 0.1 C. The capacity is stabilized at 870 mA h g^{-1} after 100 cycles with a capacity retention of 88.6%. An excellent capacity retention of ≈80% is achieved after long 800 cycles at 0.5 C by using full cell technology. Further, our post-mortem analysis sheds light on the difference in SEI layer formation on hard carbon anodes with changing electrolyte concentration, thereby indicating reasons for the obtainment of a high cyclic performance with 1 M LiTFSI salt electrolyte. The successful demonstration of the long cyclic performance of Li–polysulfide full cells is indeed a step towards producing high performance Li–polysulfide full cell batteries with long cycling using conventional LiTFSI salt electrolyte and commercial anode materials.

Introduction

The development of high-performance rechargeable batteries is very much essential to meet the ever increasing energy demand for various sectors, such as personal electronic devices, electric vehicles, and large-scale energy storage.[1–5] The rechargeable lithium–sulfur (Li–S) battery is a promising high energy density storage technology, as the elemental sulfur delivers a theoretical capacity of 1675 mA h g^{-1} and an energy density of ~2600 Wh kg^{-1} with the additional merits of being low cost, earth-abundant, relatively nontoxic, and environmentally benign.[6–8] However, there are a multitude of issues such as the inherent poor electrical conductivity of sulfur, dissolution of intermediate lithium polysulfides (LiPSs), and large volumetric change during charge–discharge cycling, which hinders the commercialization of Li–S technology.[9–11] Over decades, there have been strenuous efforts to address these issues to improve the performance of the Li–S batteries including the composite sulfur electrodes by integrating with conductive carbon materials or conducting polymers designing new architectures to buffer the volumetric expansion/shrinkage and modifying the electrode to confine the lithium polysulfides suppressing the shuttling effect.[7, 12–20]

To enhance the practical energy density of Li–S batteries, strenuous efforts are focused on the rational design of sulfur cathodes or functional electrochemically active electrolytes which can increase the cell capacity significantly.[21–23] However, the cycle life of the Li–S battery is limited with the greater sulfur loading or high areal capacity due to the critical issues of polysulfide shuttling and instability of lithium/electrolyte interfaces causing the fast electrolyte depletion and anode degradation.[22, 24] One of the crucial challenges of the development of Li–S batteries is its use of metallic lithium as an anode that has critical issues including chemical reactivity in electrolyte and dendrite growth of lithium during cycling leading to safety issues and poor cycling performance. The most recent research focuses on the positive (sulfur) electrode, with the electrolyte and Li electrode used in vast excess. However, the reports on the negative electrode and associated electrolyte degradation are scarce, decreasing our understanding of the limitations in the energy density and cycling stability. Thus, alternative negative electrode materials receive much attention in the construction of high-performance Li–S batteries. The various materials include alloys lithium–tin alloys, silicon. and graphite.[25–30] However, Si- and Sn-based alloys still undergo a large volume change, for example, an unstable interface similar to metallic lithium. On the other hand, graphite has already been successfully utilized in commercial Li–ion batteries for decades. The backbones of layered carbon frameworks have an insufficient volume change during intercalation/de-intercalation of Li$^+$ ions and establish a stable interface between graphite and the electrolyte. These critical features of graphite

[a] S. A. Ahad, Prof. S. H. Joo, Prof. H.-W. Lee
School of Energy and Chemical Engineering
Ulsan National Institute of Science and Technology (UNIST)
Ulsan 44919 (Republic of Korea)
E-mail: hyunwooklee@unist.ac.kr

[b] S. A. Ahad, Prof. R. Pitchai, Dr. A. M. Beyene, Prof. D. K. Kim
Department of Materials Science and Engineering
Korea Advanced Institute of Science and Technology
Daejeon 34141 (Republic of Korea)
E-mail: dkkim@kaist.ac.kr

[c] Prof. R. Pitchai
Electrochemical Power Sources Division, Fuel Cells Section
Central Electrochemical Research Institute
Karaikudi-630 003 (India)
E-mail: ragupathyp@cecri.res.in

Supporting Information and the ORCID identification number(s) for the author(s) of this article can be found under: https://doi.org/10.1002/cssc.201801432.

are expected to be more beneficial in Li–S batteries due to the minimum volume expansion of the graphite. However, it is well known that ethylene carbonate (EC) is incompatible with polysulfides and/or sulfur radicals generated during cycling of Li–S batteries.[31] Hard carbon is a more appealing anode with high capacity as a random alignment of small-dimensional graphene layers renders significant porosity to accommodate lithium.[32]

There are very few reports on a full cell utilizing polysulfide as the only active material. For instance, Lee et al. have reported a lithium–sulfur full cell using a dual-type (solid sulfur–polysulfide catholyte) sulfur cathode and a lithiated Si-SiO_x nanosphere anode.[3] Carbide-derived carbon (DUT-107) with a high surface area (2088 $m^2 g^{-1}$) and high total pore volume (3.17 $cm^3 g^{-1}$) is used as a rigid scaffold for sulfur infiltration to construct full cells Li–S batteries with an excellent rate cycling stability.[33] Recently, Bhargav et al. have demonstrated a graphite-polysulfide full cell with a significant capacity and cycle-life of the cells.[29] However, all the methods mentioned above involve tedious processes and utilize expensive materials. Apart from the couple of strategies mentioned above involving Li–S full cell demonstration, the effect of concentrated electrolytes especially in the Li–polysulfide full cell battery is not much studied. The effect of the concentrated electrolyte is mostly studied for lithium metal anodes aimed to improve the anode stability during the cell operation.[34] To shed light on the behavior of Li–polysulfide full cells in the presence of concentrated electrolytes, we have demonstrated a proof of concept Li–polysulfide full cell battery using 1 and 4 M lithium bis(trifluoromethanesulfonyl)imide (LiTFSI) electrolytes. The full cell constructed with glass-fiber cathode and lithiated hard carbon anode enabled us to achieve a high capacity and significant cycling stability. To the best of our knowledge, this is the first report demonstrating the use of a glass-fiber cathode and lithiated hard carbon anode in Li–polysulfide full cells with further study of the effect of electrolyte concentration on the cyclic performance. Very interestingly, the usage of inbuilt MnO_2 on a glass-fiber matrix provides a strong adsorption to polysulfides to reduce the shuttle effect. As per our previous report, the glass fiber (GF) provided a 3D network with ample space to accommodate significant amounts of polysulfides, whereas MnO_2 and multi-walled carbon nanotubes (MWCNT) provided polysulfide trapping and electrical conductivity, respectively.[7] It is well documented that concentrated electrolytes lessen the solubility of polysulfides in Li–S batteries due to Le Chatelier's Principle.[35,36] Therefore, we have also tested our system in both 1 and 4 M LiTFSI concentrated electrolyte to check their effect on the cyclic performance of a glass-fiber cathode in both half and full cells. Although the concentrated electrolyte may lessen the sulfur dissolution, its poor ionic conductivity adversely affected the specific capacity of both half- and full cell systems as compared to the conventional electrolyte. Our results show that in addition to the above mentioned benefits of our cathode system, the reduced cost and higher ionic conductivity of using conventional electrolyte are added advantages of using our proposed system for the commercialization of Li–S batteries.

Results and Discussion

Most of the carbon–sulfur composite cathodes for reasonable high capacity and significant cycling stability involve sophisticated and long processes with respect to synthesis and fabrication of the electrodes. With our previous experience on glass fibers as cathode materials for Li–polysulfide batteries, we intended to construct the Li–polysulfide full cell by utilizing glass fiber and hard carbon as the cathode and anode, respectively. The electrochemical performance of two half-cells was investigated in detail before fabricating the Li–polysulfide full cells. The galvanostatic charge–discharge cycling, cyclic, CV, and electrochemical impedance spectroscopy (EIS) of GF/MWCNT/MnO_2/Li_2S_8 cathode were carried out at two different concentrations of electrolyte, that is, 1 M LiTFSI + 0.25 M $LiNO_3$ and 4 M LiTFSI + 0.25 M $LiNO_3$ in dioxolane (DOL)/dimethoxyethane (DME) solvents. Hereafter the electrolyte compositions will be referred to as 1 M LiTFSI and 4 M LiTFSI. The present study is conducted by adding a known amount of polysulfide solution (0.5 M Li_2S_8) on the cathode substrate which is equivalent to 3 mg cm^{-2} sulfur loading.

Figure 1 shows the CV, EIS, and galvanostatic charge–discharge cycling of GF/CNT/MnO_2/Li_2S_8 obtained in 1 and 4 M LiTFSI. The CV voltammograms of GF/CNT/MnO_2/Li_2S_8 electrodes show two redox couples for both 1 and 4 M indicating the two-step reduction of sulfur. Interestingly, the peak position and peak current density are significantly different in both electrolytes clearly revealing the variation in discharge capacity. The cathodic peaks of the GF/CNT/MnO_2/Li_2S_8 electrode shifts from 2.33 to 2.21 V and from 1.93 to 1.86 V by increasing the electrolyte concentration from 1 to 4 M LiTFSI (Figure 1a). The corresponding charge–discharge curves are shown in Figure S1, Supporting Information. This potential shift is mainly attributed to the polarization of the cell. Moreover, broader anodic/cathodic peaks suggest the sluggish electrochemical reaction in 4 M LiTFSI electrolyte. The initial discharge capacities with 1 and 4 M LiTFSI electrolytes were found to be 1274 and 1211 mA h g^{-1}, respectively (Figure 1c). The high cathodic/anodic peak current density obtained with 1 M LiTFSI electrolyte is evidence of the high specific capacity compared to 4 M LiTFSI. Upon further cycling, a discharge capacity of 850 mA h g^{-1} was obtained after 100 cycles with 1 M LiTFSI electrolyte with an average coulombic efficiency of 99%. However, when the cell cycled in 4 M LiTFSI electrolyte, the discharge capacity dropped significantly to 489 mA h g^{-1} after 100 cycles. Interestingly, the discharge capacity of the GF/CNT/MnO_2/Li_2S_8-Li cell with 1 M LiTFSI showed a much more stable cycling performance as compared to 4 M LiTFSI. To verify the effect of electrolyte concentration, half cells with 2 and 3 M LiTFSI electrolyte concentrations were also tested. The cyclic performance shown in Figure S2a (Supporting Information) shows that with increasing electrolyte concentration, the discharge capacity significantly drops. To understand the variation in the capacity with different concentrations of electrolytes, the EIS analysis was performed on the fresh cells in 1 and 4 M LiTFSI. The Nyquist plots presented in Figure 1b, mainly show two semicircles in the higher and middle frequency range. The

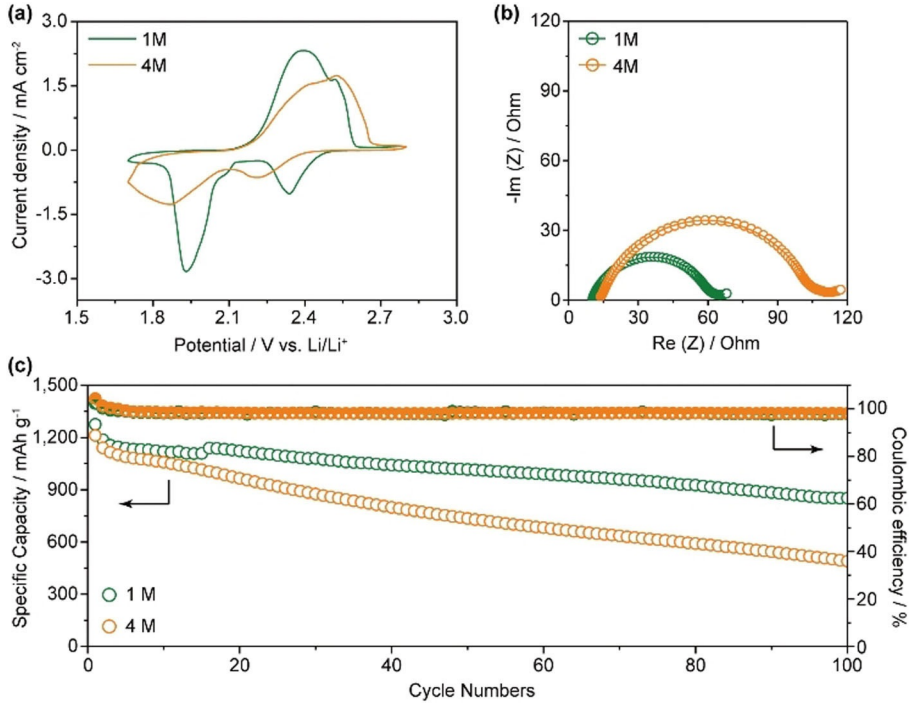

Figure 1. a) CV analysis at 0.1 mV s^{-1}; b) EIS analysis before cycling; c) Cyclic performance at 0.1 C of GF/MWCNT/MnO_2/Li_2S_8–Li half cell cycled between 2.8–1.7 V with 1 and 4 M LiTFSI electrolyte.

intercept of the semicircle at high frequency arises due to the solution resistance, the resistance of current collector, and active materials (ohmic resistance: R_o). The EIS data were fitted using the equivalent circuit given in Figure S3, Supporting Information. The solution resistances (R_o) of 1 and 4 M LiTFSI electrolyte were calculated to be 10.14 and 12.39 Ohm, respectively (Table S1, Supporting Information). The difference in the R_o values can be ascribed to the different ionic conductivity of the electrolytes. When we measured the ionic conductivity of both electrolytes, the 4 M LiTFSI electrolyte exhibits low ionic conductivity (5.86 mS cm^{-1}) compared to the 1 M LiTFSI electrolyte (11.65 mS cm^{-1}) as is also reflected in the R_o values. The ionic conductivity values of electrolytes measured using the ionic conductivity probe, summarized in Table S2, Supporting Information, also show that with increasing LiTFSI salt concentration, the ionic conductivity of the electrolyte decreases. The semicircle in the high frequency range results from the resistance (R_s) due to a passive film on the electrode surfaces, whereas the semicircle in the lower frequency range results from the charge-transfer resistance (R_{ct}) at the electrode/electrolyte interface.[33] The smaller R_{ct} value of 5.14 Ohm was obtained with 1 M LiTFSI as compared to a much higher value of 30.95 Ohm obtained with 4 M LiTFSI. A similar trend was also observed in R_s values with 1 and 4 M LiTFSI electrolyte. Although it has been reported that usually a high concentration of electrolyte increases the capacity stabilization of the Li–S battery by inhibiting polysulfide dissolution, the results suggest that the ion-transport property is a more dominant factor relative to reductive/oxidative stability by using highly concentrated electrolytes in the GF/CNT/MnO_2/Li_2S_8 electrodes, which is also consistent with some previous reports in which they did not seriously consider this poor cyclic performance.[36–39]

To demonstrate a more practical consideration of a Li–S full cell, we intend to construct a full cell of Li–polysulfide in 1 M LiTFSI by utilizing a glass-fiber composite cathode and pre-lithiated hard carbon as an anode. We have previously demonstrated that the glass-fiber-based composite cathode exhibits a high capacity and stable capacity retention.[7] To avoid dendrite growth on lithium metal, we have used pre-lithiated hard carbon as an alternative anode to metallic lithium, which demonstrates a high and stable cycling performance. Figure 2 depicts the SEM image, powder XRD pattern, and electrochemical performance of hard carbon. The irregular shaped, micron-sized particles with smooth surfaces are evident from SEM analysis. The average size of the particles ranges between 10–15 μm as shown in Figure 2a. The XRD pattern shown in Figure 2b contains two broad peaks at 23.27 and 43.81°, corresponding to (002) and (100), respectively. The (002) and (100) signifies the presence of a graphene-like structure and disordered carbon structure, respectively. The d-spacing and crystallite size of the predominant diffraction peak from (002) are 0.38 and 0.64 nm, respectively, calculated using the Scherrer equation. The large d-spacing from (002) can be beneficial in the rapid intercalation/de-intercalation of Li ions during the cycling process.[40]

With an aim to ascertain the electrochemical performance of pre-lithiated hard carbon, galvanostatic charge–discharge and cycling studies were carried out in 1 M LiTFSI electrolyte. The charge–discharge curves obtained at various cycles are shown in Figure 2c. The profile shows the typical lithiation/de-lithia-

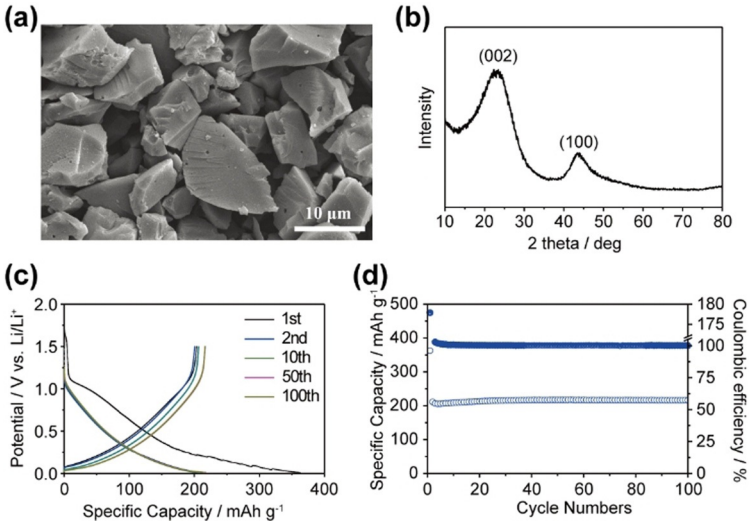

Figure 2. a, b) SEM image and XRD spectra of commercial hard carbon. c, d) Charge–discharge curve and cyclic performance of commercial hard carbon lithiated between 0.01–1.5 V at 0.5 mA cm^{-2} using 1 M LiTFSI electrolyte.

tion behavior of a hard carbon anode. The voltage plateau near 1.2–0.2 V and below 0.1 V represents the lithium intercalation between disordered graphene sheets and lithium adsorption on the pore surfaces.[41] The initial capacity of hard carbon was obtained to be 362.7 mA h g^{-1} at a current density of 0.5 mA cm^{-2}. The high capacity in the first cycle is mainly attributed to the formation of a stable SEI layer and also due to the decomposition of electrolyte on the hard carbon surface. Subsequently, the discharge capacity decreases to 210 mA h g^{-1} in the 2nd cycle. However, the nearly 100% Coulombic efficiency obtained after the 2nd cycle shows that the irreversible capacity loss has been well accommodated from the second cycle onwards. As shown in Figure 2d, the hard carbon lithiated between 1.5 V^{-1}0 mV using 1 M LiTFSI electrolyte delivered a stable discharge capacity of 216 mA h g^{-1} whilst maintaining a Coulombic efficiency of over 99% for up to 100 cycles. However, unlike graphite, the XRD comparison of hard carbon and lithiated hard carbon (Figure S4, Supporting Information) didn't show any peak shift in the XRD analysis primarily because of the significant amorphous nature of hard carbon. Some Li-oxide impurities can be located that might be due to the decomposition of electrolyte solvents at low voltage. Similar XRD analysis regarding lithiated hard carbon has been reported earlier.[42] However, the main evidence of hard carbon reversible lithiation/de-lithiation can be obtained from its charge–discharge curve discussed earlier in Figure 2c. Here it is worth mentioning that the stable lithiation capacity retention achieved in the hard carbon anode with 1 M LiTFSI electrolyte has been unsuccessful with the graphite anodes as referred to in earlier reports.[43,44] With the enhanced capacity of both half cells by a glass-fiber cathode and hard carbon anode, a full cell was assembled using GF/MNCNT/MnO_2/Li_2S_8 as a cathode and pre-lithiated hard carbon as an anode.

The CV and charge–discharge curves of the full cell are shown in Figure 3a,b. The CV of the full cell exhibits multiple cathodic peaks at 2.28, 1.90, and 1.69 V as seen in Figure 3a, whereas a major anodic peak at 2.40 V was noticed in 1 M LiTFSI. Interestingly, broad anodic/cathodic peaks in 4 M LiTFSI clearly indicate the sluggish kinetics of the redox reactions due to severe polarization resulting in a low specific capacity.[38] Further validation of the CV results can be obtained by closely observing the initial charge–discharge curve of full cells shown in Figure 3b. The corresponding charge–discharge curve shows a sharper two-step reduction process of sulfur with 1 M LiTFSI electrolyte, whereas this two-step reduction is less pronounced with 4 M LiTFSI electrolyte as evident in the CV test as well. Further, the relatively larger ΔE in the 4 M LiTFSI full cell as compared to the 1 M LiTFSI full cell also suggests higher potential polarization as the LiTFSI salt concentration increases thereby again seconding the results obtained in the CV test (Figure 3a). The initial capacities of the full cell with 1 and 4 M LiTFSI electrolyte are found to be 970 and 713 mA h g^{-1}, respectively. With 1 M LiTFSI electrolyte, a stabilized capacity of 870 mA h g^{-1} was obtained after 100 cycles at 3 mg cm^{-2} sulfur loading with an average Coulombic efficiency of 98.8%. The discharge capacity achieved in this system after 100 cycles with conventional 1 M LiTFSI electrolyte is better than the earlier reports for which either the concentrated electrolyte or other electrolyte solvents (i.e. BTFE) were introduced in the system to boost the full cell performance.[43,44] As expected, a low discharge capacity of 560 mA h g^{-1} was obtained with 4 M LiTFSI electrolyte after 100 cycles. A high capacity retention of 88.6% was achieved with 1 M LiTFSI electrolyte as compared to a low capacity retention of 78.6% with 4 M LiTFSI (Figure 3c). The capacity fading per cycle with 1 M LiTFSI and 4 M LiTFSI is 0.10 and 0.21% per cycle, respectively. Further the full cells tested with 2 and 3 M LiTFSI electrolytes showed a similar trend, which was observed while testing half cells with different electrolyte concentration, that is, with increasing electrolyte concentration the discharge capacity decreases (Figure S2b, Supporting Information). Here it is worth mentioning that the rate of capacity decay in full cells is much lower than the rate of capacity decay in the half cell systems. It is for the same reason that Li–S full cells are conceptualized to avoid rapid capacity decay on half cells that occurs due to the Li metal reaction with the electrolyte and also with lithium polysulfide species.[44] The EIS analysis of the full cells before and after 100 cycles is also presented in Figure 3d to further understand the variation in the capacity retention. The resistance values are tabulated in Table S1 (Supporting Information). As expected, the R_o and R_{ct} increases as the concentration of electrolyte used in the full cell increases. The solution resistance (R_o) of the full cell in 1 M LiTFSI before and after cycling remains almost the same whereas the R_0 value with 4 M LiTFSI electrolyte slightly increases. In both 1 and 4 M LiTFSI electrolyte containing full cells, the R value slightly decreases after cycling, thereby suggesting the formation of a stable SEI layer on the electrode surfaces. Moreover, the R_{ct} value obtained in 1 M LiTFSI slightly decreases from 4.029 Ohm before cycling to 3.658 Ohm after

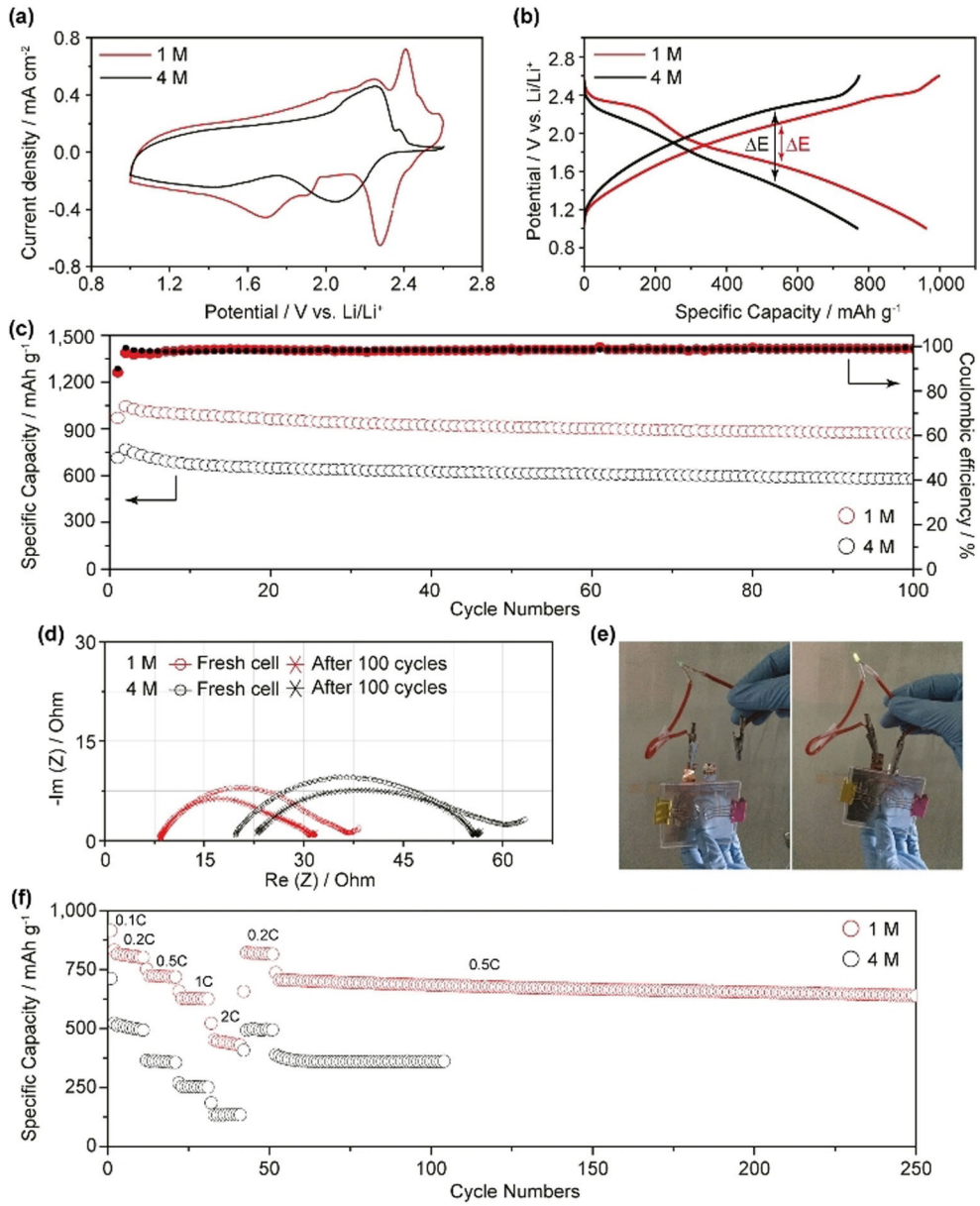

Figure 3. a) CV analysis at 0.1 mV s^{-1}; b,c) charge–discharge capacity curve and corresponding cyclic performance at 0.1 C; d) EIS analysis before cycling and after 100 cycles in the charged state; e) pouch cell demonstration with 1 M LiTFSI electrolyte lighting up a green LED; f) rate capability at various C-rates of GF/MWCNT/MnO_2/Li_2S_8–lithiated hard carbon full-cell (coin cell configuration) cycled between 2.6–1.0 V with 1 and 4 M LiTFSI electrolyte.

100 cycles, thus signifying the improved charge transfer kinetics in the full cell. However, the R_{ct} value of the full cell with 4 M LiTFSI electrolyte increases from 9.746 Ohm before cycling to 14.08 Ohm after 100 cycles. Here, the increase in the R_{ct} resistance reflects reduced charge-transfer kinetics which results in the lower discharge capacity and cycling performance in the full cell containing 4 M LiTFSI electrolyte. As discussed earlier in the half cell, the high R_{ct} value in the full cell may be due to the lower ionic conductivity of the concentrated electrolyte. Further, the GF/MWCNT/MnO_2/Li_2S_8–lithiated hard carbon pouch cell using 1 M LiTFSI electrolyte was fabricated. As shown in Figure 3 e, the lighting up of the LED can be seen once the connections are made with the GF/MWCNT/MnO_2/Li_2S_8–lithiated hard carbon pouch cell. We believe that such a demonstration shows the potential of Li–polysulfide full cells to be scaled up for use in commercial applications. Further, with an aim to investigate the electrochemical reversibility and feasibility for the practical applications, a rate capability test was carried out using a coin cell setup and data is shown in Figure 3 f. The discharge capacities of a full cell containing 1 M LiTFSI electrolyte were found to be 915.2, 831.7, 751.4, 658.2, and 521.7 mA h g^{-1} at 0.1, 0.2, 0.5, 1, and 2 C, respectively. Once the cell was subjected again to a low C-rate of 0.2 C, it gains the full discharge capacity indicating the excellent reversibility and rate performance. Moreover, when the cell was subjected to a high C-rate of 0.5 C, a capacity of 702.9 and 640.4 mA h g^{-1} was obtained after 100 and 250 cycles, which corresponds to 93.5 and 85.3 % capacity retention, respectively.

The corresponding voltage-specific capacity curve shows a typical and well defined two-voltage plateau at all C-rates thus reaffirming the robust rate performance of the full cell in 1 M LiTFSI electrolyte (Figure S5 a, Supporting Infprmation). As expected, inherently lower capacity values were obtained with 4 M LiTFSI electrolyte (Figure 3 f, Figure S5 b, Supporting Information). When the GF/MWCNT/MnO_2-Li_2S_8 full cell with 1 M LiTFSI electrolyte (Figure S6, Supporting Information) was subjected to a long cycling test at a current density of 0.5 C, it delivered a capacity of 818 and 650 mA h g^{-1} after the 1st and 800th cycles, respectively, with a columbic efficiency of 99.5 %. The capacity retention after 800 cycles was ≈80 %. The successful demonstration of a long cyclic performance of a Li–polysulfide full cell is indeed a step towards producing a high-performance Li–polysulfide full cell battery with long cycling using a hard carbon anode material.

Finally, the post mortem analysis of the full cell was performed by extracting the cathode and the anode after 100 cycles, cycled at 0.1 C. Figure 4 a confirms that the intertwined structure of the cathode remains intact after long cycling. Also, the deposition of solid sulfur can be seen on the cathode surface. It is worth mentioning that even after the deposition of solid sulfur a lot of pores can be seen in the cathode in which a large amount of lithium polysulfides can be accommodated during cycling. The energy dispersive spectroscopy (EDS) analysis of the cathode revealed uniform deposition of sulfur on the cathode surface along with the presence of carbon and oxygen (Figure 4 b). Similar results were obtained in the cathode extracted from the full cell containing 4 M LiTFSI electrolyte (Figure S7, Supporting Information). Before performing SEM, a crack was deliberately created in the cathode structure to analyze the internal structure of the cath-

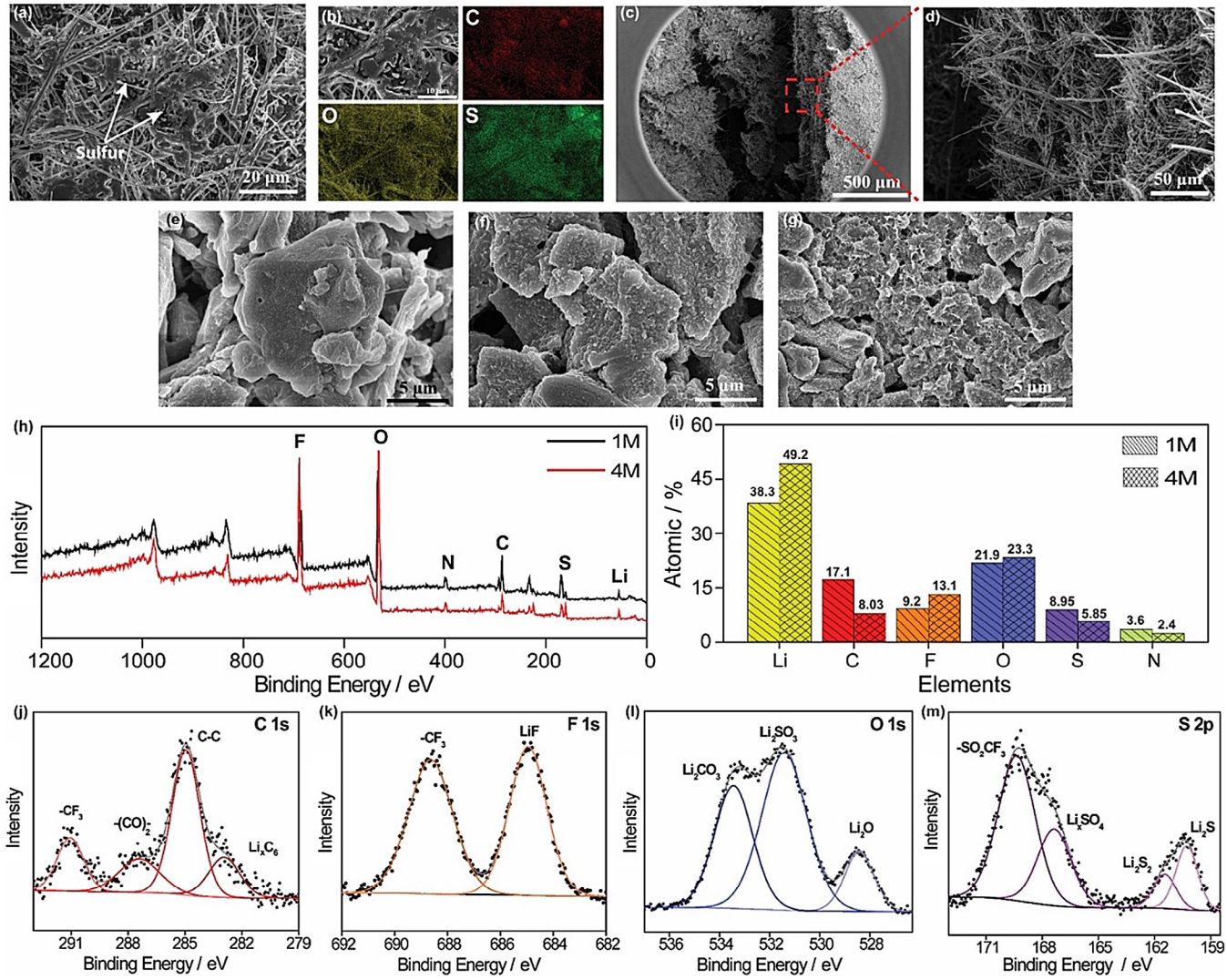

Figure 4. a, b) SEM image and corresponding EDS analysis [C: carbon (red), O: oxygen (yellow), S: sulfur (green)] of the cycled cathode after 100 cycles at 0.1 C in the charged state extracted from GF/MWCNT/MnO_2/Li_2S_8–lithiated hard carbon full-cell with 1 M LiTFSI electrolyte; c, d) SEM images of the intentionally induced crack in cathode showing porous spaces inside the cathode architecture. SEM images of cycled anode extracted after 100 cycles at 0.1 C in the charged state from GF/MWCNT/MnO_2/Li_2S_8–lithiated hard carbon full-cell; e) with 1 M LiTFSI electrolyte; f, g) with 4 M LiTFSI electrolyte; h, i) XPS survey spectrum and corresponding atomic percentage of elements present in the cycled hard carbon anode extracted from full cells containing 1 and 4 M LiTFSI electrolyte. j–m) C 1s, F 1s, O 1s, and S 2p spectrum of cycled anode extracted from a full cell containing 1 M LiTFSI electrolyte.

ode (Figure 4c). The zoomed area of the cracked region shows that a lot of porous regions are present in the GF/MWCNT/MnO_2 substrate that can accommodate more active material during further cycling (Figure 4d). This robust architecture of the cathode has enabled us to achieve a high specific capacity from a Li–S full cell. Similar post-mortem analysis was carried out on the anode surface. As presented in Figure 4e and Figure S8, Supporting Information, the SEM image shows uniform deposition of a secondary electrolyte interface (SEI) layer on the hard carbon anode extracted after an initial lithiation of 5 cycles (later used to construct full cells with 1 and 4 M LiTFSI electrolyte) and from the full cell with 1 M LiTFSI electrolyte after 100 cycles. On the contrary, the anode extracted from the full cell with 4 M LiTFSI electrolyte shows coarser and nonuniform deposition of the SEI layer (Figure 4f,g). It is observed that the SEI layer deposited on the hard carbon particles is primarily the decomposition product of LiTFSI electrolyte, $LiNO_3$ additive, and lithium polysulfides that migrated towards the anode.[45,46] The corresponding EDS mapping of the anodes is shown in Figure S9 and S10, Supporting Information. In the SEI layer, the C, O, F, and S comes from the reduced solvents, products from $LiNO_3$ decomposition, reduction products from LiTFSI salt, and lastly from reduced lithium polysulfides.[47,48] In addition, the voltage range (2.6–1.0 V) used in this study to investigate the full cell might have further promoted the decomposition of $LiNO_3$ during cycling.[49] The EDS analysis presented in Figure S11, Supporting Information, shows that the atomic percentage of carbon (C) has decreased since the concentrated electrolyte will have less contribution from the decomposition of solvent. However, the higher atomic percentage of oxygen (O) and fluorine (F) present in the full cell with 4 M LiTFSI electrolyte as compared to the full cell with 1 M LiTFSI electrolyte suggests that with 4 M LiTFSI, a greater amount of SEI components get deposited on the lithiated hard carbon anode; this is because the highly concentrated LiTFSI salt tends to deposit more reduced products on the anode surface. The analysis was further supported by performing XPS on the cycled anodes. The survey spectrum and the corresponding atomic percentages (Figure 4h,i, Figure S12c–h, Supporting Information) shows a higher atomic percentage of Li, F, and O on the cycled anode extracted from the full cell containing 4 M LiTFSI electrolyte thereby confirming higher LiTFSI salt decomposition and deposition on its surface as compared to 1 M LiTFSI electrolyte. On the other hand, the C atomic percentage is higher in the cycled anode of the full cell with 1 M LiTFSI electrolyte because of the increased 'solvent' decomposition as compared to concentrated 4 M LiTFSI electrolyte (higher concentration of salt in a given volume of solvent) in which more 'salt' decomposition takes place. The individual analysis of elemental spectra of the cycled anode from a full cell with 1 M LiTFSI electrolyte is summarized in Figure 4j–m and Table S3 (Supporting Information). The C 1s spectrum explains that the SEI layer contains products from decomposed solvent (C–C), PAA binder (–CO_2–), and LiTFSI salt (–CF_3–).[50,51] Another peak appearing at 282.6 eV comes from the lithiated carbon (Li_xC_6) which disappears in the case of cycled anode from 4 M LiTFSI electrolyte (Figure S12c, Supporting Information). This suggests that the SEI layer formed on the cycled anode with 4 M LiTFSI electrolyte is much thicker as compared to the layer formed due to 1 M LiTFSI electrolyte.[52] Further analysis of the F, O, S, N, and Li spectrum confirms the presence of LiF, Li_2SO_3, –SO_2CF_3, Li_xSO_4, N^- (TFSI), and Li_3N peaks, which arise due to the decomposition of LiTFSI salt. Peaks such as Li_2O, Li_2CO_3, and $ROCO_2Li$ are due to the reaction of Li salt with the DOL/DME solvents. The S 2p spectra also shows the presence of Li_2S/Li_2S_2 polysulfides that might have migrated towards the anode and reduced on its surface.[53,54] The dense SEI layer on the anode may have retarded the charge-transfer process in the lithiated anode during full cell battery operation, thereby providing low specific capacity from the full cell in 4 M LiTFSI. This hypothesis can be further explained by revisiting the EIS data presented in Figure 3c and Table S2 (Supporting Information). The charge-transfer resistance (R_{ct}) in the case of the full cell with 1 M LiTFSI after 100 cycles is much lower than with 4 M LiTFSI, which further strengthens the claim that the dense SEI layer formed on the anode with 4 M LiTFSI is not favorable to drive high capacity in the Li–polysulfide full cell setup.

Conclusions

In summary, we have successfully demonstrated the Li–polysulfide full cell constructed from glass-fiber-based composites as a cathode and pre-lithiated hard carbon as the anode, respectively. Further, the electrolyte study suggests that 1 M LiTFSI electrolyte is the most suitable for obtaining high specific capacity due to its high ionic conductivity as compared to the other concentrated LiTFSI electrolyte. The Li–polysulfide full cell delivers the initial discharge capacity of 970 mA h g^{-1} at 0.1 C. Further, the capacity of the full cell stabilized at 870 mA h g^{-1} after 100 cycles using conventional 1 M LiTFSI electrolyte. The higher ionic conductivity and the uniform deposition of the SEI layer on the cycled anode with 1 M LiTFSI electrolyte helped it to perform better as compared to concentrated electrolytes in the Li–polysulfide full cell. We believe that the present work may open a new platform for the construction of a novel combination of cathode and anode materials for Li–sulfur/Li–polysulfide batteries by using conventional LiTFSI electrolyte systems.

Experimental Section

All experimental details can be found in the Supporting Information.

Acknowledgements

P. R. is thankful to the Korean Federation of Science and Technology Societies for financial support through the Brain Pool Program and Dr. V. K. Pillai, Director, CSIR-CECRI, for his support and granting him the sabbatical leave. This project was supported by the National Research Foundation of Korea (NRF) (MSIP) (No. 2017R1A2B2010148) and the Climate Change Research Hub of EEWS from KAIST (Grant No. N11170059). H.-W. L. acknowledges

support from the Individual Basic Science & Engineering Research Program (NRF-2016R1C1B2013935) and Basic Research Lab Program (NRF-2017R1A4A1015533) through the NRF funded by MSIT.

Conflict of interest

The authors declare no conflict of interest.

Keywords: concentrated electrolyte · full cells · lithium–sulfur batteries · polysulfide · SEI layer

[1] P. G. Bruce, S. A. Freunberger, L. J. Hardwick, J.-M. Tarascon, *Nat. Mater.* **2012**, *11*, 19 – 29.
[2] A. Manthiram, Y. Fu, S. H. Chung, C. Zu, Y. S. Su, *Chem. Rev.* **2014**, *114*, 11751 – 11787.
[3] S. K. Lee, S. M. Oh, E. Park, B. Scrosati, J. Hassoun, M. S. Park, Y. J. Kim, H. Kim, I. Belharouak, Y. K. Sun, *Nano Lett.* **2015**, *15*, 2863 – 2868.
[4] Z. Li, J. Zhang, B. Guan, D. Wang, L.-M. Liu, X. W. (David) Lou, *Nat. Commun.* **2016**, *7*, 13065.
[5] J. Zhang, Y. Shi, Y. Ding, W. Zhang, G. Yu, *Nano Lett.* **2016**, *16*, 7276 – 7281.
[6] Z. Liang, G. Zheng, W. Li, Z. W. Seh, H. Yao, K. Yan, D. Kong, Y. Cui, *ACS Nano* **2014**, *8*, 5249 – 5256.
[7] P. Ragupathy, S. A. Ahad, P. R. Kumar, H.-W. Lee, D. K. Kim, *Adv. Sustainable Syst.* **2017**, *1*, 1700083.
[8] S. A. Ahad, P. Ragupathy, S. Ryu, H.-W. Lee, D. K. Kim, *Chem. Commun.* **2017**, *53*, 8782 – 8785.
[9] S. Evers, L. F. Nazar, *Acc. Chem. Res.* **2013**, *46*, 1135 – 1143.
[10] S. A. Ahad, P. R. Kumar, J.-H. Kim, P. Ragupathy, D. K. Kim, D. J. Kim, *Electrochim. Acta* **2017**, *246*, 451 – 458.
[11] S. Moon, Y. H. Jung, D. K. Kim, *J. Power Sources* **2015**, *294*, 386 – 392.
[12] L. Borchardt, H. Althues, S. Kaskel, *Curr. Opin. Green Sustainable Chem.* **2017**, *4*, 64 – 71.
[13] Z. Zhang, L. L. Kong, S. Liu, G. R. Li, X. P. Gao, *Adv. Energy Mater.* **2017**, *7*, 1 – 12.
[14] G. Li, J. Sun, W. Hou, S. Jiang, Y. Huang, J. Geng, *Nat. Commun.* **2016**, *7*, 10601.
[15] S. Zeng, L. Li, L. Xie, D. Zhao, N. Wang, S. Chen, *ChemSusChem* **2017**, *10*, 4829 – 4832.
[16] X. Ye, J. Ma, Y.-S. Hu, H. Wei, F. Ye, *J. Mater. Chem. A* **2016**, *4*, 775 – 780.
[17] S. Moon, Y. H. Jung, W. K. Jung, D. S. Jung, J. W. Choi, D. K. Kim, *Adv. Mater.* **2013**, *25*, 6547 – 6553.
[18] H. Du, Z. Zhang, J. He, Z. Cui, J. Chai, J. Ma, Z. Yang, C. Huang, G. Cui, *Small* **2017**, *13*, 1702277.
[19] T. Ma, F. Zhou, T. W. Zhang, H. Bin Yao, T. Y. Su, Z. L. Yu, Y. Li, L. L. Lu, S. H. Yu, *Angew. Chem. Int. Ed.* **2017**, *56*, 11836 – 11840; *Angew. Chem.* **2017**, *129*, 11998 – 12002.
[20] F. Zhou, Z. Li, X. Luo, T. Wu, B. Jiang, L. L. Lu, H. Bin Yao, M. Antonietti, S. H. Yu, *Nano Lett.* **2018**, *18*, 1035 – 1043.
[21] G. Zhou, L. Li, C. Ma, S. Wang, Y. Shi, N. Koratkar, W. Ren, F. Li, H. M. Cheng, *Nano Energy* **2015**, *11*, 356 – 365.
[22] D. Lv, J. Zheng, Q. Li, X. Xie, S. Ferrara, Z. Nie, L. B. Mehdi, N. D. Browning, J. G. Zhang, G. L. Graff, J. Liu, J. Xiao, *Adv. Energy Mater.* **2015**, *5*, 1402290.
[23] F. Zhou, L. T. Song, L. L. Lu, H. Bin Yao, S. H. Yu, *ChemNanoMat* **2016**, *2*, 937 – 941.
[24] Y. Ma, H. Zhang, B. Wu, M. Wang, X. Li, H. Zhang, *Sci. Rep.* **2015**, *5*, 14949.
[25] J. Hassoun, B. Scrosati, *Angew. Chem. Int. Ed.* **2010**, *49*, 2371 – 2374; *Angew. Chem.* **2010**, *122*, 2421 – 2424.
[26] R. Elazari, G. Salitra, G. Gershinsky, A. Garsuch, A. Panchenko, D. Aurbach, *Electrochem. Commun.* **2012**, *14*, 21 – 24.
[27] J. Brückner, S. Thieme, F. Böttger-Hiller, I. Bauer, H. T. Grossmann, P. Strubel, H. Althues, S. Spange, S. Kaskel, *Adv. Funct. Mater.* **2014**, *24*, 1284 – 1289.
[28] S. Zheng, Y. Chen, Y. Xu, F. Yi, Y. Zhu, Y. Liu, J. Yang, C. Wang, *ACS Nano* **2013**, *7*, 10995 – 11003.
[29] A. Bhargav, M. Wu, Y. Fu, *J. Electrochem. Soc.* **2016**, *163*, A1543 – A1549.
[30] Z. Hu, S. Zhang, C. Zhang, G. Cui, *Coord. Chem. Rev.* **2016**, *326*, 34 – 85.
[31] M. Cuisinier, C. Hart, M. Balasubramanian, A. Garsuch, L. F. Nazar, *Adv. Energy Mater.* **2015**, *5*, 1401801.
[32] T. Zheng, J. S. Xue, J. R. Dahn, *Chem. Mater.* **1996**, *8*, 389 – 393.
[33] S. Thieme, J. Brueckner, A. Meier, I. Bauer, K. Gruber, J. Kaspar, A. Helmer, H. Althues, M. Schmuck, S. Kaskel, *J. Mater. Chem. A* **2015**, *3*, 3808 – 3820.
[34] J. Qian, W. A. Henderson, W. Xu, P. Bhattacharya, M. Engelhard, O. Borodin, J.-G. Zhang, *Nat. Commun.* **2015**, *6*, 6362.
[35] L. Suo, Y.-S. Hu, H. Li, M. Armand, L. Chen, *Nat. Commun.* **2013**, *4*, 1481.
[36] E. S. Shin, K. Kim, S. H. Oh, W. Il Cho, *Chem. Commun.* **2013**, *49*, 2004 – 2006.
[37] S. Urbonaite, P. Novák, *J. Power Sources* **2014**, *249*, 497 – 502.
[38] Y. Z. Zhang, S. Liu, G. C. Li, G. R. Li, X. P. Gao, *J. Mater. Chem. A* **2014**, *2*, 4652.
[39] J. W. Choi, J. K. Kim, G. Cheruvally, J. H. Ahn, H. J. Ahn, K. W. Kim, *Electrochim. Acta* **2007**, *52*, 2075 – 2082.
[40] J. Zhang, X. Liu, J. Wang, J. Shi, Z. Shi, *Electrochim. Acta* **2016**, *187*, 134 – 142.
[41] R. Alcántara, G. F. Ortiz, P. Lavela, J. L. Tirado, R. Stoyanova, E. Zhecheva, *Chem. Mater.* **2006**, *18*, 2293 – 2301.
[42] D. Hirshberg, D. Sharon, E. De La Llave, M. Afri, A. A. Frimer, W.-J. Kwak, Y.-K. Sun, D. Aurbach, *ACS Appl. Mater. Interfaces* **2017**, *9*, 4352 – 4361.
[43] S. Chen, Z. Yu, M. L. Gordin, R. Yi, J. Song, D. Wang, *ACS Appl. Mater. Interfaces* **2017**, *9*, 6959 – 6966.
[44] D. Lv, P. Yan, Y. Shao, Q. Li, S. Ferrara, H. Pan, G. L. Graff, B. Polzin, C. Wang, J.-G. Zhang, J. Liu, J. Xiao, *Chem. Commun.* **2015**, *51*, 13454 – 13457.
[45] D. Aurbach, E. Pollak, R. Elazari, G. Salitra, C. S. Kelley, J. Affinito, *J. Electrochem. Soc.* **2009**, *156*, A694 – A702.
[46] X. B. Cheng, R. Zhang, C. Z. Zhao, F. Wei, J. G. Zhang, Q. Zhang, *Adv. Sci.* **2015**, *3*, 1 – 20.
[47] H. Kim, J. T. Lee, G. Yushin, *J. Power Sources* **2013**, *226*, 256 – 265.
[48] S. Zhang, K. Ueno, K. Dokko, M. Watanabe, *Adv. Energy Mater.* **2015**, *5*, 1 – 28.
[49] S. S. Zhang, *Electrochim. Acta* **2012**, *70*, 344 – 348.
[50] M. R. Busche, T. Drossel, T. Leichtweiss, D. A. Weber, M. Falk, M. Schneider, M. L. Reich, H. Sommer, P. Adelhelm, J. Janek, *Nat. Chem.* **2016**, *8*, 426 – 434.
[51] N. W. Li, Y. X. Yin, J. Y. Li, C. H. Zhang, Y. G. Guo, *Adv. Sci.* **2017**, *4*, 1600400.
[52] Y. Pan, G. Wang, B. L. Lucht, *Electrochim. Acta* **2016**, *217*, 269 – 273.
[53] S. Xiong, K. Xie, Y. Diao, X. Hong, *J. Power Sources* **2013**, *236*, 181 – 187.
[54] S. Xiong, K. Xie, Y. Diao, X. Hong, *J. Power Sources* **2014**, *246*, 840 – 845.

Manuscript received: June 26, 2018
Accepted manuscript online: July 27, 2018
Version of record online: August 23, 2018